THE JOURNAL OF PHYSICAL CHEMISTRY B

Article

pubs.acs.org/JPCB

Magneto-LC Effects in Hydrogen-Bonded All-Organic Radical Liquid Crystal

Yoshiaki Uchida,*[,†] Katsuaki Suzuki,[‡] and Rui Tamura[‡]

[†]Graduate School of Engineering Science, Osaka University, 1-3 Machikaneyama-cho, Toyonaka, Osaka 560-8531, Japan

[‡]Graduate School of Human and Environmental Studies, Kyoto University, Yoshida-Nihonmatsu-cho, Sakyo-ku, Kyoto 606-8501, Japan

Supporting Information

ABSTRACT: To identify the origin of the magneto-LC effects, which refer to the enhancement of intermolecular magnetic interactions in the LC phases of all-organic radical compounds, we have designed and synthesized H-bonded all-organic radical compounds showing nematic and cholesteric phases for the first time. They show stronger magneto-LC effects than in the same LC phases of analogous covalent-bonded all-organic radical LC compounds. Variable-temperature electron paramagnetic resonance spectroscopy of the hydrogen-bonded compounds reveals that the inhomogeneous intermolecular contacts give rise to the magneto-LC effects.

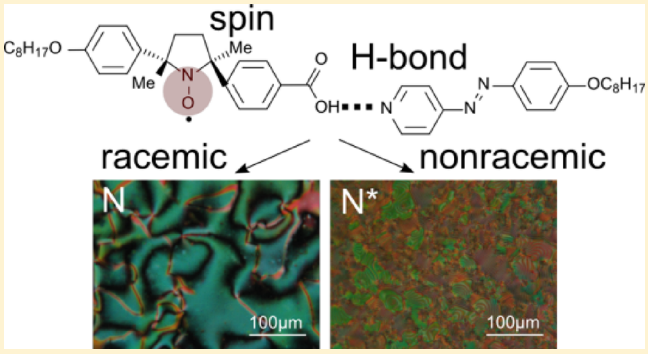

1. INTRODUCTION

Paramagnetic liquid crystalline (LC) compounds attract a great deal of attention because of their fascinating properties in externally applied fields.[1−3] For example, their molecular reorientation in a uniform magnetic field[4,5] and the motion of magnetic LC droplet in a magnetic field gradient have been reported.[6] Furthermore, their magnetic susceptibility is known to be sensitive to an applied electric field.[7] One fascinating property is the magneto-LC effects, which refers to the enhancement of intermolecular magnetic interactions in LC phases.[8,9] The magneto-LC effects were detected for the first time as an abrupt increase in magnetic susceptibility at the crystalline (Cr)-to-LC phase transition of a nitroxide radical LC compound.[8] The understanding of the origin of the magneto-LC effects is important for the design of molecules showing larger magnetic susceptibility or even all-organic ferromagnetic LC materials. Thus, the mechanism leading to specific intermolecular magnetic interactions in LC phases remains to be completely elucidated.[8−10] We previously proposed that the inhomogeneity of intermolecular contacts in LC phases is one of the factors of the effects.[8]

It has been reported that, when a covalent bond in the mesogen core is replaced with a hydrogen bond, orientational order parameter (S) decreases.[11,12] The decrease of the orientational order in LC phases leads to more inhomogeneity of the intermolecular contacts. Accordingly, a nitroxide radical LC compound with such a hydrogen bond in the core region should show lower S in LC phases than covalent-bonded compounds, and then, the disordering may enhance the inhomogeneity of the intermolecular contacts. Therefore, such a hydrogen-bonded (H-bonded) nitroxide radical LC compound must give us important information about the relationship between the magneto-LC effects and the inhomogeneous intermolecular contacts.

Here, we report the synthesis of the first example of all-organic radical LC compounds with a hydrogen bond in the mesogen core. The magnto-LC effects of the H-bonded nitroxide radical LC compounds are evaluated by means of variable-temperature electron paramagnetic resonance (VT-EPR) spectroscopy. Furthermore, we have developed a novel method to discuss the influence of the inhomogeneous intermolecular contacts in detail using EPR spectra.

2. EXPERIMENTAL SECTION

2.1. Syntheses and Characterization. Nitroxide radical carboxylic acid (**1**), a hydrogen-bond donor for H-bonded LC compounds, is exhibited in Figure 1. We synthesized racemic **1** (rac-**1**) and (2*S*,5*S*)-enriched **1** (ss-**1**) according to a previously reported procedure.[13] As a hydrogen-bond acceptor, we selected molecule **2** with a pyridyl group (Figure 1).[14] The synthetic procedure for compound **2** is described in the Experimental Section.[15] Racemic and enantio-enriched complexes of **1** and **2** (rac-**3** and ss-**3**) were obtained from a chloroform solution containing equimolar amounts of a carboxyl group and pyridine moiety. In the infrared (IR) spectra of rac-**3**, the absorption bands corresponding to the H-bonded O−H stretching vibration of the carboxyl groups were observed at 2481 and 1907 cm^{-1}. In the IR spectra of ss-**3**, the

Received: February 27, 2012
Revised: July 6, 2012
Published: July 19, 2012

dx.doi.org/10.1021/jp301930k | *J. Phys. Chem. B* 2012, 116, 9791−9795

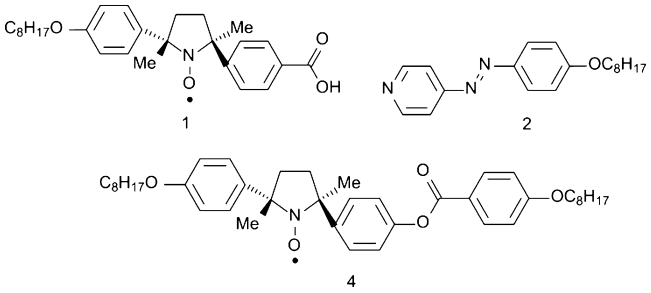

Figure 1. Molecular structures of **1**, **2**, and **4**.

absorption bands corresponding to the H-bonded O−H stretching vibration of the carboxyl groups were observed at 2503 and 1893 cm^{-1}. In contrast, in the single carboxylic acids rac-**1** and ss-**1**, there was no absorption resulting from the hydrogen bonding.

2.1.1. Materials. All reagents were used without further purification. ^1H NMR spectra were recorded using a JNM-ECX400 (JEOL). ESI-mass were recorded with microTOF II (Bruker)

2.1.2. Synthesis of 4-(4-Hydroxyphenylazo)pyridine. 4-Aminopyridine (3.0 g, 32 mmol) was dissolved in 25 mL of hydrochloric acid (7 N), and the resulting solution was cooled to 0 °C. With stirring, a mixture of 2.0 g (29 mmol) of sodium nitrite, 2.5 g (27 mmol) of phenol, and sodium hydroxide (25 mmol) in water (20 mL) was added dropwise into the solution to produce diazonium salt. The reaction mixture was stirred at 0 °C for 2 h. After sodium hydroxide was added to the reaction mixture to give pH 7, the precipitated solid was collected and extracted with ethyl acetate. The extracts were washed with water, dried over $MgSO_4$, and filtered. After the solvent was removed, 4-(4-hydroxyphenylazo)pyridine (1.3 g, 9 mmol) was obtained in 28% yield.

^1H NMR (CD_3OD, 400 MHz): δ = 6.93 (d, J = 9 Hz, 2H), 7.74 (d, J = 6 Hz, 2H), 7.88 (d, J = 9 Hz, 2H), 8.64 (d, J = 6 Hz, 2H). MS (ESI) Found: m/z = 200.0818 $[M+1]^+$ (199.0739 calc. for $C_9H_9N_3O$)

*2.1.3. Synthesis of 4-(4-Octyloxyphenylazo)pyridine (**2**).* To a stirred solution of 4-(4-hydroxyphenylazo)pyridine (500 mg, 2.5 mmol) and K_2CO_3 (524 mg 3.8 mmol) in dimethylformamide (15 mL) was added bromooctane (482 mg, 2.5 mmol). The reaction mixture was stirred at 70 °C for 6 h, poured into water, and then extracted by hexane.

The extracts were washed with sat. $NaHCO_3$, NaOH, and brine and dried over $MgSO_4$. After the solvent was removed, the crude products were purified by column chromatography on silica gel (hexane/dichloromethane = 1:1) to give **2** (505 mg, 1.6 mmol) in 65% yield.

^1H NMR (CD3Cl, 400 MHz): δ = 0.90 (t, J = 5 Hz, 3H), 1.24−1.41 (m, 8H), 1.49 (q, J = 8 Hz, 2H), 1.83 (q, J = 7 Hz, 2H), 4.06 (t, J = 7 Hz, 2H), 7.02 (d, J = 9 Hz, 2H), 7.67 (d, J = 6 Hz, 2H) 7.95 (d, J = 9 Hz, 2H), 8.77 (d, J = 6 Hz, 2H). MS (ESI) found: m/z = 312.2075 $[M+1]^+$(311.1991 calc. for $C_{17}H_{25}N_3O$).

*2.1.4. Supramolecular Complexes (rac-**3**, ss-**3**).* The supramolecular complexes of the carboxylic acids rac-**1** and ss-**1** and the phenylazopyridine **2** were synthesized by a procedure in the main text of ref 5. rac-**1** (0.030 mmol) or ss-**1** (0.017 mmol) and **2** (0.030 or 0.017 mmol) were dissolved in chloroform (200 μL), and each mixture was slowly evaporated at 60 °C at normal pressures and then the chloroform was completely removed in vacuo.

2.2. Measurements. The X-band EPR spectra were measured under an applied magnetic field of 0.33 T. Five measurements were performed at each temperature. Sweep time was 150 s. Sample was sealed in a glass tube with Ar gas. The variable temperature XRD patterns were recorded at a continuous scanning rate of 2° 2θ min^{-1} at heating and cooling rates of 4 °C min^{-1} using Cu Kα radiation (40 kV, 20 mA), with the intensity of the diffracted X-rays being collected at intervals of 0.02° 2θ. DSC was performed at a scanning rate of 5 °C min^{-1}.

3. RESULTS AND DISCUSSION

3.1. Phase Transition Behavior. The phase transition behavior is confirmed by differential scanning calorimetry (DSC), polarized optical microscopy (POM; Figure 2), and X-ray diffraction (XRD) measurements. All of the ingredients, rac-**1**, ss-**1**, and **2**, are nonmesogenic compounds (Table 1). In contrast, DSC charts for rac-**3** and ss-**3** indicate that the complexes formed from nonmesogenic components show LC

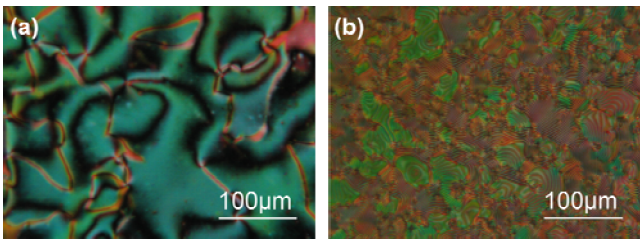

Figure 2. Optical polarized micrographs showing (a) the Schlieren texture at 105.0 °C of rac-**3** and (b) the fingerprint texture at 120.0 °C of (2*S*,5*S*)-**3** in the cooling run.

Table 1. Phase Transition Behavior of 1, 2, and 3 Determined by DSC Analysis

	phase transition temperarutes (°C) (ΔH (kJ mol^{-1}))	
rac-**1**	Cr 156.3 (-)[a] Iso	heating
ss-**1**	Cr 135.2 (12.2) Iso	heating
2	Cr 57.3(0.7) Iso	heating
rac-**3**	Cr 121.7 (32.5) Iso	second heating
	Iso 117.5 (3.3) N 91.3 (27.4) Cr	second cooling
ss-**3**	Cr 113.4 (27.4) N* 135.3 (4.0) Iso	second heating
	Iso 133.9 (4.2) N* 101.7 (27.0) Cr	second cooling

[a]It is impossible to measure the enthalpy because decomposition occurs in association with melting.

Scheme 1. Synthesis of Compound 2

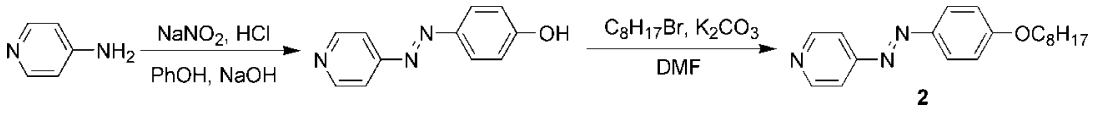

dx.doi.org/10.1021/jp301930k | J. Phys. Chem. B 2012, 116, 9791−9795

phases (Figure S1). XRD measurements for the LC phases gave no peak. rac-**3** showed a Schlieren texture typical for a nematic (N) phase by POM (Figure 2a), whereas ss-**3** (>99% ee) exhibited a fingerprint texture characteristic of a cholesteric (N*) phase (Figure 2b). Thus, the LC phases of rac-**3** and ss-**3** can be identified as a monotropic N phase (in the cooling run) and an enantiotropic N* phase, respectively. This mesophase stabilization can be ascribed to the effect of the highly planar structure of the phenylazopyridine unit, which is a core unit of the H-bonded mesogen.

3.2. Temperature Dependence of Magnetic Susceptibility. To confirm whether the H-bonded LC compounds show magneto-LC effects, we performed VT-EPR spectroscopy for rac-**3** between 80 and 135 °C and for ss-**3** between 90 and 145 °C in a magnetic field of 0.33 T (X-band) by using a quartz tube (5 mm ϕ). To evaluate paramagnetic susceptibility from the EPR spectra by previously reported method,[8] we fitted the experimental data to the differential Lorentzian function[16]

$$I'(H) = -16I'_{\mathrm{m}}\frac{H - H_0}{\Delta H_{\mathrm{pp}}/2}\Big/\left\{3 + \left(\frac{H - H_0}{\Delta H_{\mathrm{pp}}/2}\right)^2\right\}^2 \quad (1)$$

where I'_{m} is the maximum peak height of the differential curve, H is the applied magnetic field, H_0 is the resonant magnetic field, and ΔH_{pp} is the peak-to-peak line width. To discuss the weak effects by using accurately measured data, EPR spectra were measured in the narrow range of magnetic field as shown in Figure S2. Meanwhile, the line widths are so wide that the lines protrude outside the range of magnetic field. Thus, even if the EPR peaks are double-integrated, the paramagnetic susceptibility cannot be accurately estimated. Without the double-integration, we can easily evaluate the paramagnetic susceptibility (χ) from the parameters I'_{m}, H_0, and ΔH_{pp} by eq 2.[8]

$$\chi = \frac{2\mu_{\mathrm{B}}gI'_{\mathrm{m}}\Delta H_{\mathrm{pp}}{}^2}{\sqrt{3}\,h\nu H_1} \quad (2)$$

where μ_{B} is the Bohr magneton, h is Planck's constant, ν is the frequency of the absorbed electromagnetic wave, g is the g factor, which is inversely proportional to H_0, and H_1 is the amplitude of the oscillating magnetic field (see the Supporting Information). The temperature dependence of relative paramagnetic susceptibility (χ_{rel}), which is defined as

$$\chi_{\mathrm{rel}} = \frac{\chi}{\chi_0} \quad (3)$$

where χ_0 is the standard paramagnetic susceptibility at 90 °C in the heating run, for rac-**3** and ss-**3** is shown in Figure 3.

In the heating run, χ_{rel} abruptly increases at the melting (Cr-to-isotropic (Iso) and Cr-to-N* phase transitions) points for rac-**3** (26% increase from 110 to 125 °C) and ss-**3** (40% increase from 109 to 119 °C), respectively; it decreases with increasing temperature in each phase, as expected from the Curie–Weiss law. In the cooling run, χ_{rel} increases with decreasing temperature in the Iso and N(N*) phases, abruptly decreases at the N(N*)-to-Cr phase transition by 16% (16%) from 105 °C (98 °C) to 100 °C (95 °C), and increases with decreasing temperature in the Cr phase for rac-**3** (ss-**3**). Similar to the case of previously reported magneto-LC effects of a covalent-bonded analogue **4**,[8] a very small change in the χ_{rel} value is commonly noted at the Iso-to-LC phase transition in the cooling run.

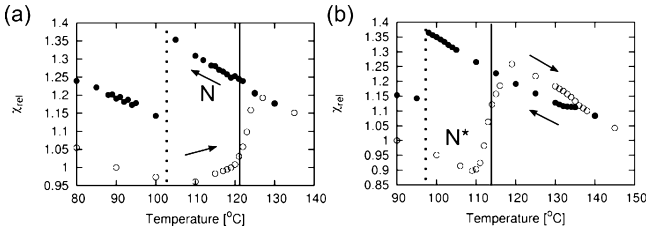

Figure 3. Temperature dependence of χ_{rel} obtained from variable temperature EPR (VT-EPR) spectroscopy (a) for rac-**3** and (b) for ss-**3**. Open and filled circles denote the data in the heating and cooling runs, respectively. Vertical solid and dotted lines denote the melting points obtained by DSC analysis in the heating run and freezing points expected by the temperature dependence of g value in the cooling run, respectively.

The abrupt χ_{rel} changes at the melting and freezing points should be attributed to the molecular paramagnetic anisotropy $\Delta\chi_{\mathrm{mol}}$ and/or the intermolecular magnetic interactions J. The contribution of $\Delta\chi_{\mathrm{mol}}$ can be expressed in terms of the change in the g value resulting from magnetic-field-induced molecular reorientation. It is well-known that χ_{rel} is proportional to g^2 when J is constant.[8] By using the experimental g values evaluated by the method described in Figure S3, however, the increases in χ_{rel} are expected to be below 0.002% at the melting and freezing points. This indicates that the $\Delta\chi_{\mathrm{mol}}$ does not contribute to the abrupt change in χ_{rel} at the melting and freezing points of rac-**3** and ss-**3**. These results suggest two possibilities; one is the case that Cr phases show antiferromagnetic interactions ($J < 0$), and the other is the case that the intermolecular magnetic interactions in the LC and Iso phases are ferromagnetic ($J > 0$).

To determine whether the magnetic interactions in the crystalline phases were antiferromagnetic, we measured the temperature dependence of the paramagnetic susceptibility in the temperature range 2–300 K in the first heating run (both rac-**3** and ss-**3** show crystalline phases in this temperature range). The data in the temperature range of 100–300 K were fitted to the Curie–Weiss law (Figure S4):

$$\chi = \frac{C}{T - \theta} \quad (4)$$

where C is a Curie constant, T is temperature, and θ is Weiss constant. C and θ were then estimated for rac-**3** (C = 0.37, θ = −0.36 K) and ss-**3** (C = 0.38, θ = 0.62 K). These results suggest that the crystalline phases do not show strong antiferromagnetic intermolecular interactions but remain paramagnetic over the temperature range. Even if the weak magnetic interactions vanish at the melting points, the change of the paramagnetic interactions are smaller than 0.25% over 400K. Thus, to explain the large increase in the paramagnetic susceptibility at the melting points (26% and 40% for rac-**3** and ss-**3**, respectively), the generation of ferromagnetic interactions in the LC phases should be assumed.

The χ_{rel} increases at the melting (Cr–N and Cr–N* phase transition) points of racemic and enantio-enriched samples of a previous reported covalent-bonded compound **4** shown in Figure 1 were 16% (from 74 to 78 °C) and 23% (from 73 to 78 °C), respectively.[8] The χ_{rel} increases at the melting points of rac-**3** and ss-**3** are apparently larger than those in the melting points of covalent-bonded compounds **4**. According to Curie–

dx.doi.org/10.1021/jp301930k | J. Phys. Chem. B 2012, 116, 9791–9795

Weiss low, the χ_{rel} increases should decrease as phase transition temperature increases (see the Supporting Information). Furthermore, the melting points of rac-**4** and ss-**4** are lower than the corresponding transition temperatures of rac-**3** and ss-**3**, respectively. Thus, the difference in the χ_{rel} increase between **3** and **4** should be larger than it looks. The intense magneto-LC effects probably result from the existence of the inhomogeneous intermolecular contacts.

3.3. VT-EPR Spectroscopy. To discuss the influence of the inhomogeneous intermolecular contacts on the magneto-LC effects, we focused on the inhomogeneous broadening of the EPR spectra. It is well-known that EPR spectra are inhomogeneously broadened by unresolved proton hyperfine coupling and magnetic-field modulation, and hence the spectra become Voigt function, which is the convolution of Gaussian with Lorentzian functions.[17] The Gaussian component of peak-to-peak line width (ΔH^{G}_{pp}) contains the contribution of unresolved proton hyperfine coupling (ΔH^{G}_{pp0}) and magnetic-field modulation (κH_m), where H_m is the modulation amplitude and κ is a constant.[16] In our case, the contribution of inhomogeneous intermolecular contacts (H_{IIC}) should be added to the Gaussian component. Therefore, ΔH^{G}_{pp} can be expressed as the sum of their squares[18]

$$\Delta H^{G\,2}_{pp} = \Delta H^{G\ 2}_{pp0} + \kappa^2 H_m{}^2 + H_{IIC}{}^2 \quad (5)$$

Among the terms, only $H_{IIC}{}^2$ depends on temperature. Thus, we can discuss the influence of inhomogeneous intermolecular contacts on the magneto-LC effects by analyzing the temperature dependence of ΔH^{G}_{pp}. Then, we fitted the spectra obtained from the numerical integration of the raw data ($I(H)$) to the Voigt function

$$I(H) = I_v \int \frac{\exp[-(H' - H_0)^2/2\sigma^2]}{1 + \left(\frac{H' - H}{\Delta H^{L}_{1/2}/2}\right)^2} dH' \quad (6)$$

where σ is equal to $\Delta H^{G}_{pp}/2$, I_V is a constant, and $\Delta H^{L}_{1/2} = (3)^{1/2}\Delta H^{L}_{pp}$, which is the Lorentzian peak-to-peak line width influenced by the magnitude of intermolecular magnetic interactions. The parameters (ΔH^{L}_{pp}, ΔH^{G}_{pp}, and g) were obtained from fitting the experimental data to eq 6 as shown in Figures 4 and S3.

Generally, intermolecular magnetic interactions are divided into two factors, (a) spin−spin exchange interactions and (b) spin−spin dipole interactions. To discuss about the contribution of the two factors the temperature dependence of ΔH^{L}_{pp} is useful.[8] When the dipole interactions increase or the exchange interactions decrease, ΔH^{L}_{pp} increases. For both complexes, in the heating run, ΔH^{L}_{pp} decreases with increasing temperature and the rate of decrease of ΔH^{L}_{pp} increases with increasing temperature up to the melting points. Subsequently, the rate decreases with increasing temperature in the Iso phases. In the cooling run, ΔH^{L}_{pp} increases with decreasing temperature in all phases and increases abruptly at the freezing points for both compounds. ΔH^{L}_{pp} decreases when χ abruptly increases at the melting points, whereas it increases when χ decreases at the freezing points (Figure 3). Accordingly, we concluded that the spin−spin exchange interactions are likely to contribute to the abrupt change in χ at the melting and freezing points. However, other effects might be responsible for the observed line broadening. This point will be studied in the near future.

The additional spin−spin exchange interactions in LC and Iso phases are supposed to arise from the inhomogeneous intermolecular contacts in the phases. Thus, we estimate the contribution of the inhomogeneity on the magnetic interactions from the temperature dependence of ΔH^{G}_{pp}. In the heating run, ΔH^{G}_{pp} is quite small in the initial Cr phases, increases slightly at the melting points, and then decreases with increasing temperature for both compounds. The increase in ΔH^{G}_{pp} and the decrease in ΔH^{L}_{pp} at the melting points in the heating run indicate the appearance of inhomogeneous spin−spin exchange interactions. In the cooling run, ΔH^{G}_{pp} increases with decreasing temperature in all phases for both compounds; further, ΔH^{G}_{pp} reaches a plateau at the freezing point for rac-**3**, whereas ΔH^{G}_{pp} abruptly decreases at the freezing point for ss-**3**. These behaviors indicate that inhomogeneous intermolecular contacts in both LC and Iso phases remain in the crystalline phases to some extent in the cooling run. In fact, we observed a difference in the ΔH^{L}_{pp} and g value in the crystalline phases between the heating and cooling runs (Figures 4 and S3). The crystal structures obtained by cooling the samples from the LC phases are likely to be different from the initial crystal structures.

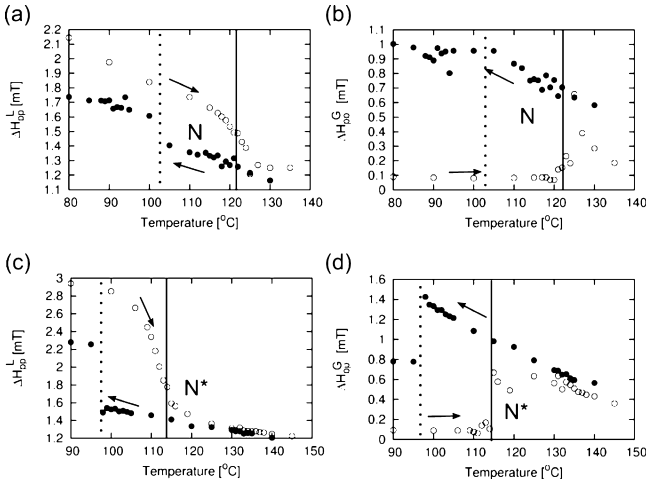

Figure 4. The temperature dependence of linewidths obtained from variable temperature EPR (VT-EPR) spectroscopy for rac-**3** and ss-**3**. Panels a and b show temperature dependence of ΔH^{L}_{pp} and ΔH^{G}_{pp} for rac-**3**, respectively, and panels c and d show temperature dependence of ΔH^{L}_{pp} and ΔH^{G}_{pp} for ss-**3**. Open and filled circles denote the data in the heating and cooling runs, respectively. Vertical solid and dotted lines denote the melting points obtained by DSC analysis in the heating run and freezing points expected by the temperature dependence of g value in the cooling run, respectively (Figure S3).

If magneto-LC effects arise from the inhomogeneous intermolecular contacts, the increase of ΔH^{G}_{pp} at the melting points for the covalent-bonded analogue **4** could be observed. We fitted the reported EPR spectra for **4**[8] to eq 6 as shown in Figure S5. In fact, at the melting points the ΔH^{G}_{pp} of **4** changes in the same direction as that of **3**, though the ΔH^{L}_{pp} of **4** changes in the opposite direction from that of **3**. The former result indicates that the inhomogeneous contacts between nitroxide radical groups should occur at the melting points for both **3** and **4**. Whereas the ΔH^{G}_{pp} increase at the melting point of rac-**4** is much smaller than that of rac-**3**, the ΔH^{G}_{pp} increase at the melting points of ss-**4** is a little larger than that of ss-**3**. Although we cannot simply compare the results because **4** has a mesogen core with fewer benzene rings than **3**, the introduction of an H-bond may tend to enhance the inhomogeneity. Meanwhile, the latter result suggests that **4** is likely to show the enhancement of spin−spin dipole interactions at the melting points as previously reported.[8] Therefore, we can conclude that

dx.doi.org/10.1021/jp301930k | J. Phys. Chem. B 2012, 116, 9791−9795

inhomogeneous intermolecular contacts should give rise to inhomogeneous intermolecular magnetic interactions, but the type of spin−spin interactions that is enhanced then is likely to depend on the molecular structure. In the present case, the introduction of an H-bond probably would result in the enhancement of the intermolecular spin−spin exchange interactions.

4. CONCLUSIONS

We synthesized the first example of racemic and nonracemic H-bonded chiral all-organic radical compounds showing N and N* phases, in which they show stronger magneto-LC effects than covalent-bonded LC compounds show. The results of VT-EPR spectroscopy imply that the magneto-LC effects arise from the inhomogeneous intermolecular contacts. Furthermore, we believe that spin−spin exchange interactions are probably responsible for the magneto-LC effects. These results indicate the possibility of a noncovalent bond being one of the key components in the synthesis of high-performance LC compounds with the following intermolecular-contact-dependent properties: conductivity,[19] color,[20] charge transfer,[21] and magnetic properties. To constitute such a principle, additional work needs to be performed.

■ ASSOCIATED CONTENT

Ⓢ Supporting Information

Additional discussions and Figures S1−S5. This material is available free of charge via the Internet at http://pubs.acs.org.

■ AUTHOR INFORMATION

Corresponding Author

*E-mail: yuchida@cheng.es.osaka-u.ac.jp. Tel: +81-6-6850-6256;. Fax: +81-6-6850-6256.

Notes

The authors declare no competing financial interest.

■ ACKNOWLEDGMENTS

This work was supported by the Grants-in-Aid for Scientific Research (Nos. 23245008 and 23655127) from Japan Society for the Promotion of Science (JSPS). Y.U. and K.S. are grateful to the JSPS Research Fellowships for Young Scientists.

■ REFERENCES

(1) Griesar, K.; Haase, W. In *Magnetic Properties of Organic Molecules*; Lahti, P. M., Ed.; Marcel Dekker: New York, 1999; Chapter 16, pp 325−344.
(2) Kaszynski, P. In *Magnetic Properties of Organic Molecules*; Lahti, P. M., Ed.; Marcel Dekker: New York, 1999; Chapter 15, pp 305−324.
(3) Tamura, R.; Uchida, Y.; Ikuma, N. *J. Mater. Chem.* **2008**, *18*, 2872−2876.
(4) Galyametdinov, Y. G.; Haase, W.; Goderis, B.; Moors, D.; Driesen, K.; Deun, R. V.; Binnemans, K. *J. Phys. Chem. B* **2007**, *111*, 13881−13885.
(5) Uchida, Y.; Tamura, R.; Ikuma, N.; Shimono, S.; Yamauchi, J.; Shimbo, Y.; Takezoe, H.; Aoki, Y.; Nohira, H. *J. Mater. Chem.* **2009**, *19*, 415−418.
(6) Uchida, Y.; Ikuma, N.; Tamura, R.; Shimono, S.; Noda, Y.; Yamauchi, J.; Aoki, Y.; Nohira, H. *J. Mater. Chem.* **2008**, *18*, 2950−2952.
(7) Suzuki, K.; Uchida, Y.; Tamura. R.; Shimono, S.; Yamauchi, J. "Observation of electric field dependence of molecular orientation and anisotropic magnetic interactions by EPR spectroscopy in the surface-stabilized liquid crystal cell of an all-organic nitroxide radical compound showing a ferroelectric SmC* phase." Manuscript submitted for publication.
(8) Uchida, Y.; Suzuki, K.; Tamura, R.; Ikuma, N.; Shimono, S.; Noda, Y.; Yamauchi, J. *J. Am. Chem. Soc.* **2010**, *132*, 9746−9752.
(9) Lee, C. H.; Kwon, Y. W.; Choi, D. H.; Geerts, Y. H.; Koh, E.; Jin, J. I. *Adv. Mater.* **2010**, *22*, 4405−4409.
(10) Suzuki, K.; Uchida, Y.; Tamura, R.; Shimono, S.; Yamauchi, J. *J. Mater. Chem.* **2012**, *22*, 6799−6806.
(11) Barmatov, E.; Grande, S.; Filippov, A.; Barmatova, M.; Kremer, F.; Shibaev, V. *Macromol. Chem. Phys.* **2000**, *201*, 2603−2609.
(12) Filippov, A. P. *J. Opt. Technol.* **2001**, *68*, 700−703.
(13) Uchida, Y.; Uematsu, T.; Nakayama, Y.; Takahashi, H.; Tsue, H.; Tanaka, K.; Tamura, R. *Chirality* **2008**, *20*, 282−287.
(14) Mallia, V. A.; Antharjanam, P. K. S.; Das, S. *Liq. Cryst.* **2003**, *30*, 135−141.
(15) Mamiya, J.; Yoshitake, A.; Kondo, M.; Yu, Y.; Ikeda, T. *J. Mater. Chem.* **2008**, *18*, 63−65.
(16) Noda, Y.; Shimono, S.; Baba, M.; Yamauchi, J.; Uchida, Y.; Ikuma, N.; Tamura, R. *Appl. Magn. Reson.* **2008**, *33*, 85−93.
(17) Bales, B. L. In *Biological Magnetic Resonance*; Berliner, L. J., Reuben, J., Eds.; Plenum Press: New York, 1989; Vol. *8*, pp 77−130.
(18) Bales, B. L.; Peric, M.; Lamy-Freund, M. T. *J. Magn. Reson.* **1998**, *132*, 279−286.
(19) Funahashi, M.; Hanna, J.-I. *Adv. Mater.* **2005**, *17*, 594−598.
(20) Sagara, Y.; Yamane, S.; Mutai, T.; Araki, K.; Kato, T. *Adv. Funct. Mater.* **2009**, *19*, 1869−1875.
(21) Araya, K.; Matsunaga, Y. *Bull. Chem. Soc. Jpn.* **1980**, *53*, 3079−3084.